nature | **methods**

Fast, high-contrast imaging of animal development with scanned light sheet–based structured-illumination microscopy

Philipp J Keller, Annette D Schmidt, Anthony Santella, Khaled Khairy, Zhirong Bao, Joachim Wittbrodt & Ernst H K Stelzer

Supplementary figures and text:

Supplementary Figure 1	DSLM-SI implementation
Supplementary Figure 2	DSLM-SI illumination patterns for the typical range of SI frequencies
Supplementary Figure 3	DSLM-SI illumination patterns for high SI frequencies
Supplementary Figure 4	Mirror surface reconstruction with DSLM-SI
Supplementary Figure 5	Imaging tissue phantoms with DSLM-SI
Supplementary Figure 6	DSLM-SI performance at low to intermediate scattering coefficients
Supplementary Figure 7	DSLM-SI performance at high scattering coefficients
Supplementary Figure 8	Contrast enhancement in Medaka DSLM-SI recordings
Supplementary Figure 9	DSLM-SI coverage in zebrafish multi-channel recordings
Supplementary Figure 10	DSLM-SI coverage at advanced zebrafish embryonic development
Supplementary Figure 11	DSLM-SI coverage at late zebrafish embryonic development
Supplementary Figure 12	Removal of scattered light in zebrafish DSLM-SI recordings
Supplementary Figure 13	Removal of scattered light in *Drosophila* DSLM-SI recordings
Supplementary Figure 14	DSLM-SI penetration depth in early *Drosophila* embryogenesis
Supplementary Figure 15	Workflow for processing and visualization of DSLM-SI recordings
Supplementary Figure 16	Multiple-view fusion of the *Drosophila* Digital Embryo
Supplementary Table 1	Properties of tissue phantoms

Note: Supplementary Videos 1–6 and Supplementary Data 1–2 are available on the Nature Methods website.

Supplementary Figure 1 | DSLM-SI implementation

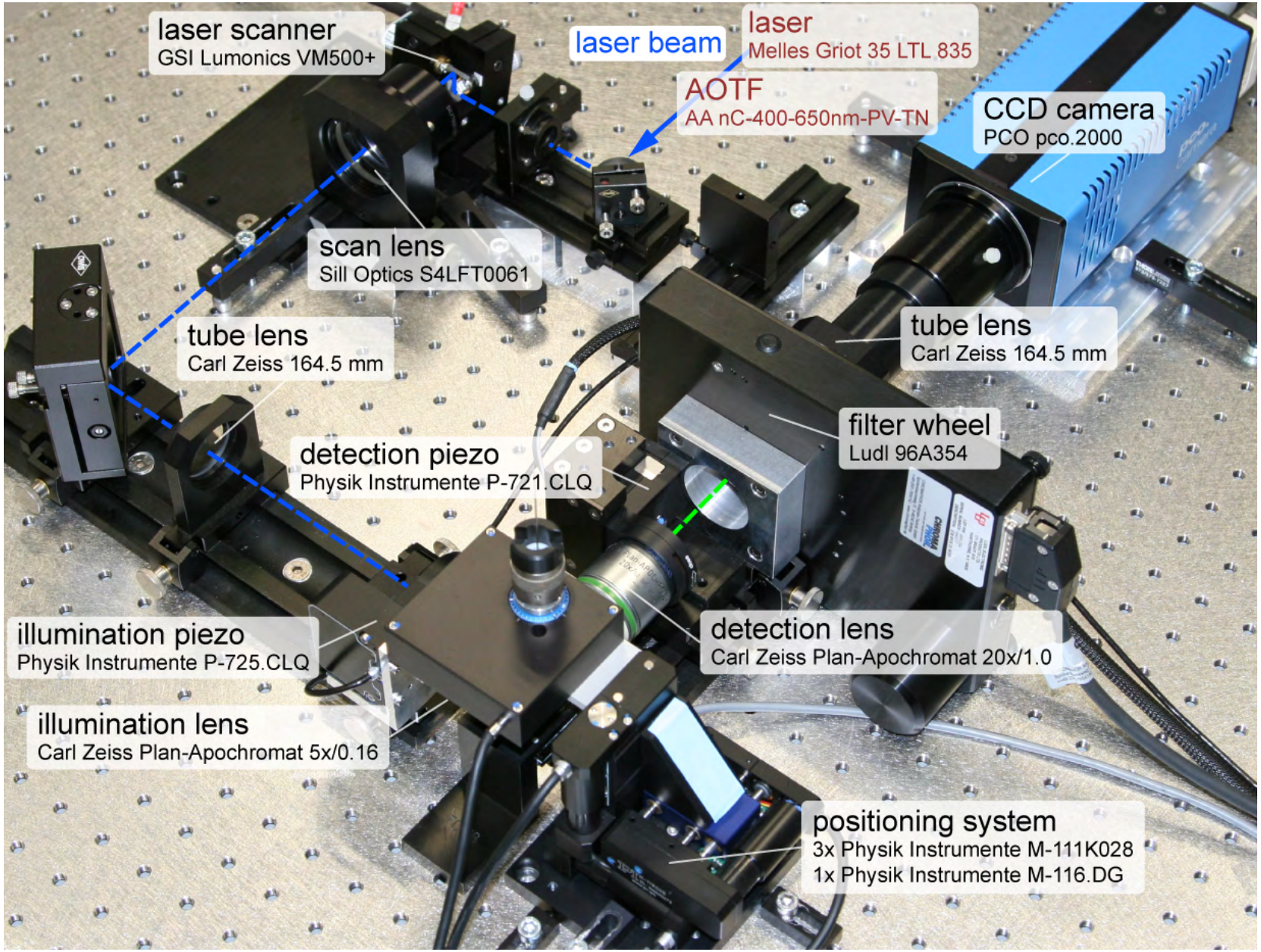

Supplementary Figure 1 | DSLM-SI implementation

Photograph of the central part of our DSLM-SI imaging platform using a single CCD camera for fluorescence detection. The figure shows the DSLM sub-systems for illumination (blue dashed line) and detection (green dashed line).

Supplementary Figure 2 | DSLM-SI illumination patterns for the typical range of SI frequencies

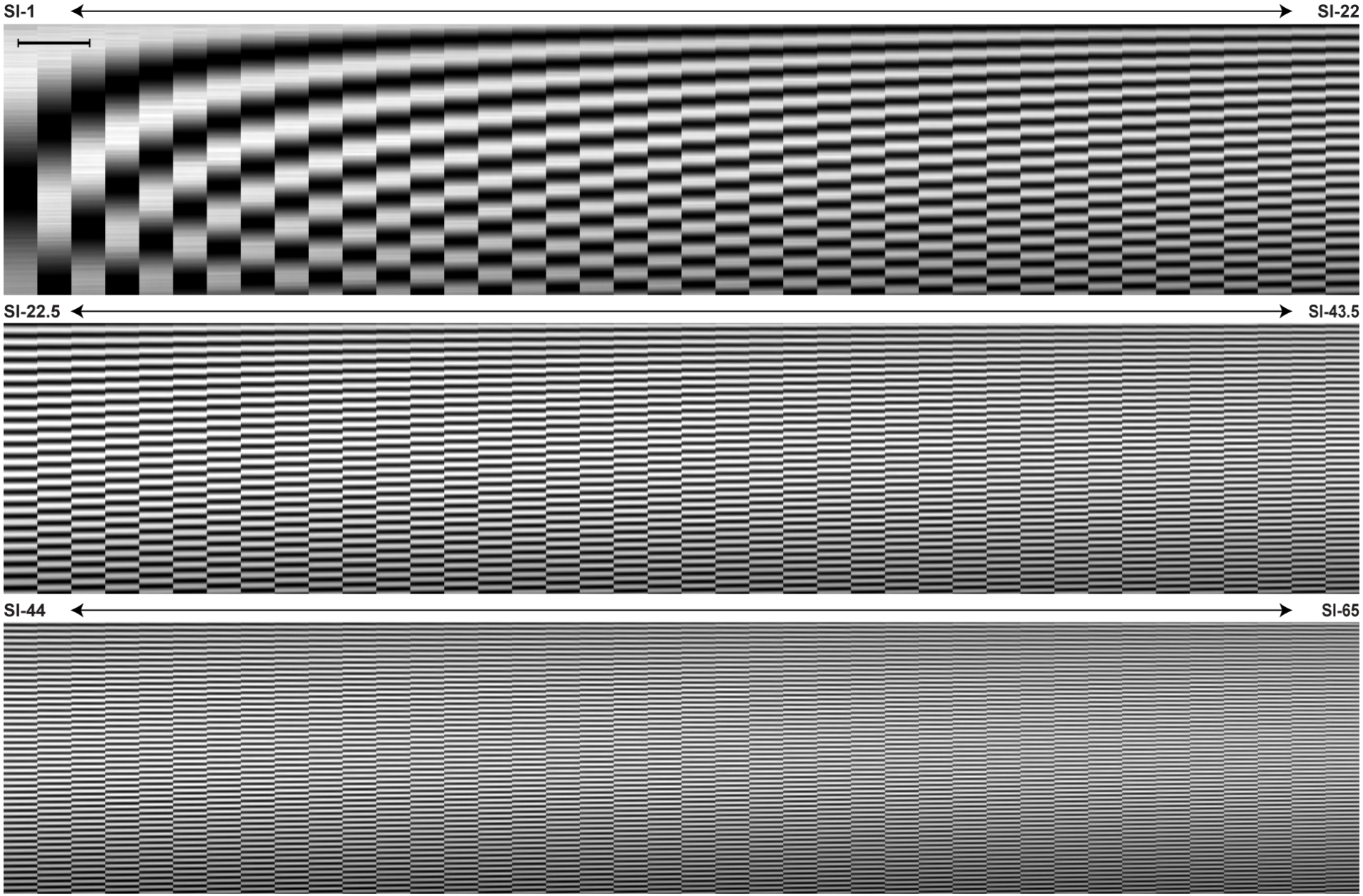

Supplementary Figure 2 | DSLM-SI illumination patterns for the typical range of SI frequencies

Microscopy recordings of DSLM-SI illumination patterns in the frequency range SI-1 to SI-65. The DSLM-SI fluorescence patterns were recorded using an agarose cylinder containing rhodamine-dextran (sample geometry as in Supplementary Figure 5a). Fluorescence levels are slightly decreased in the lower part due to diffusion of rhodamine-dextran out of the cylinder and into the water-filled sample chamber. Scale-bar = 200 µm. Carl Zeiss Plan-Apochromat 20×/1.0 W.

Supplementary Figure 3 | DSLM-SI illumination patterns for high SI frequencies

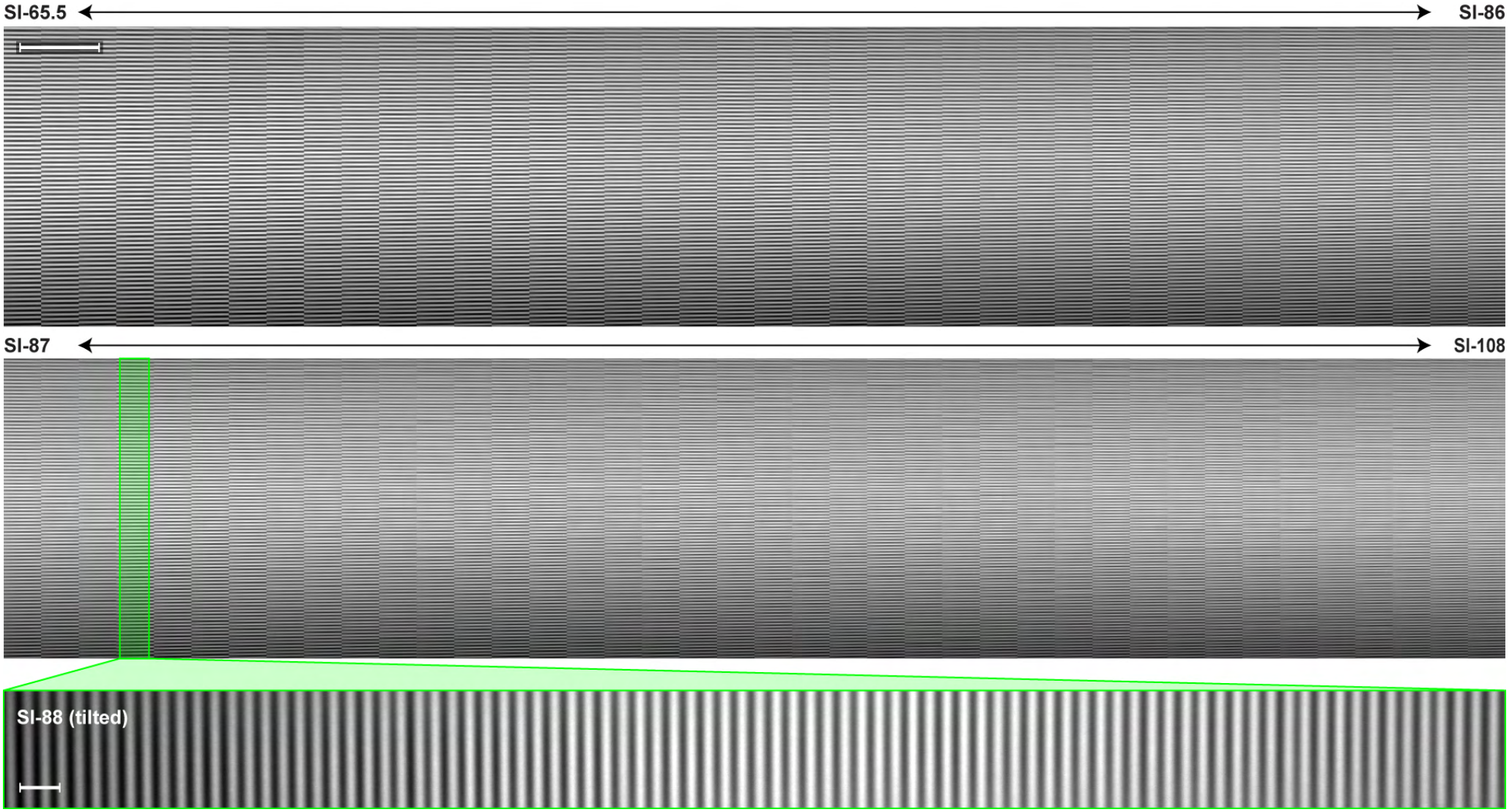

Supplementary Figure 3 | DSLM-SI illumination patterns for high SI frequencies

Microscopy recordings of DSLM-SI illumination patterns in the frequency range SI-65.5 to SI-108. This figure is an extension of the panels shown in Supplementary Figure 2. Scale-bars = 200 µm (main panel), 20 µm (close-up). Carl Zeiss Plan-Apochromat 20×/1.0 W.

Supplementary Figure 4 | Mirror surface reconstruction with DSLM-SI

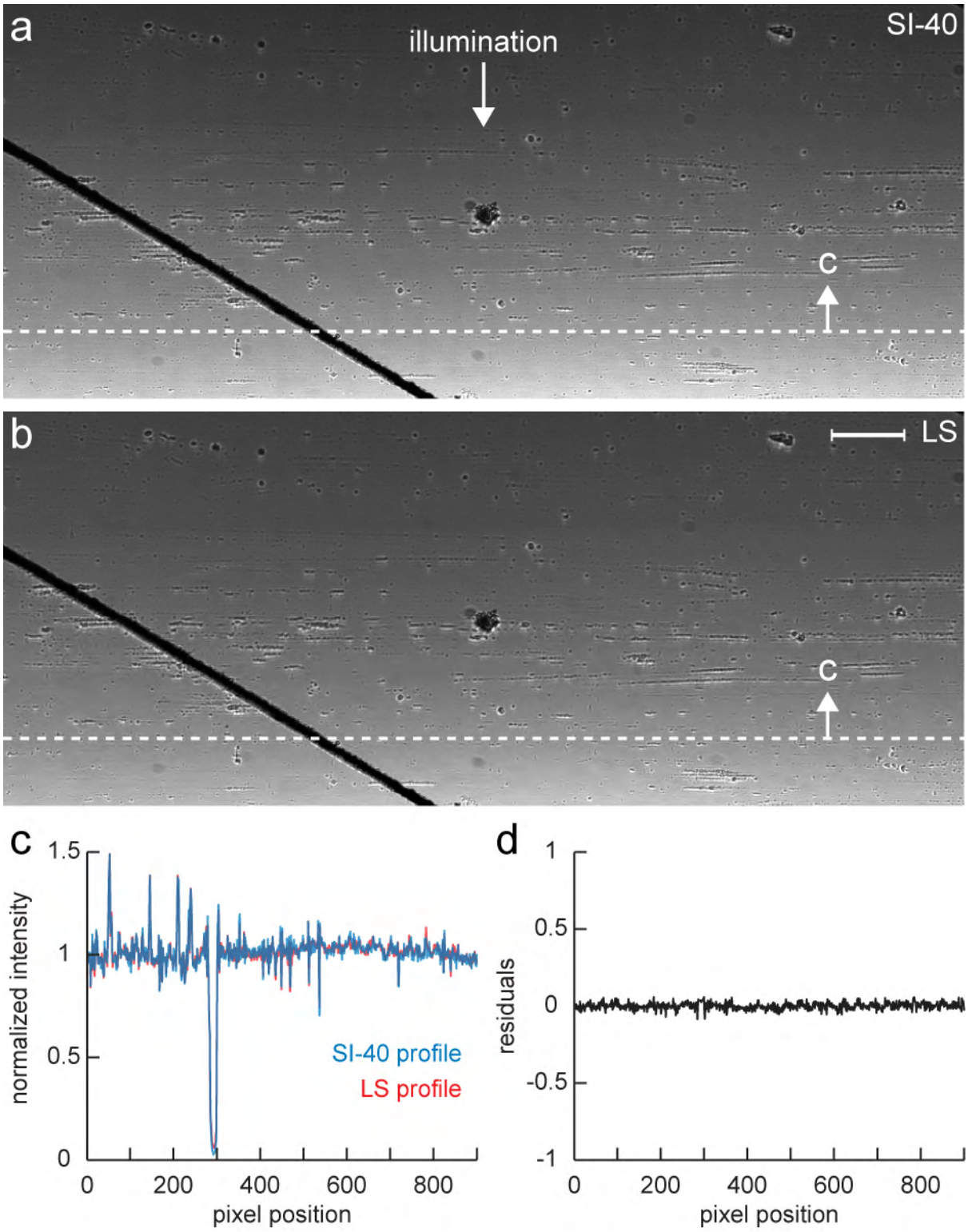

Supplementary Figure 4 | Mirror surface reconstruction with DSLM-SI

(**a**) Maximum-intensity projection of a DSLM-SI image stack showing the surface of a scratched mirror. The surface was scanned with an SI-40 illumination profile at a wavelength of 488 nm, providing a data set of 2,000 images recorded in 500 nm steps.

(**b**) Standard DSLM light sheet recording of the mirror shown in (a), using the same acquisition settings except for the illumination mode. Scale-bar = 50 µm. Carl Zeiss C-Apochromat 10×/0.45 W.

(**c**) Intensity plot along the line indicated in (a) and (b).

(**d**) Deviation of SI-40 and LS intensity profiles shown in (c).

Supplementary Figure 5 | Imaging tissue phantoms with DSLM-SI

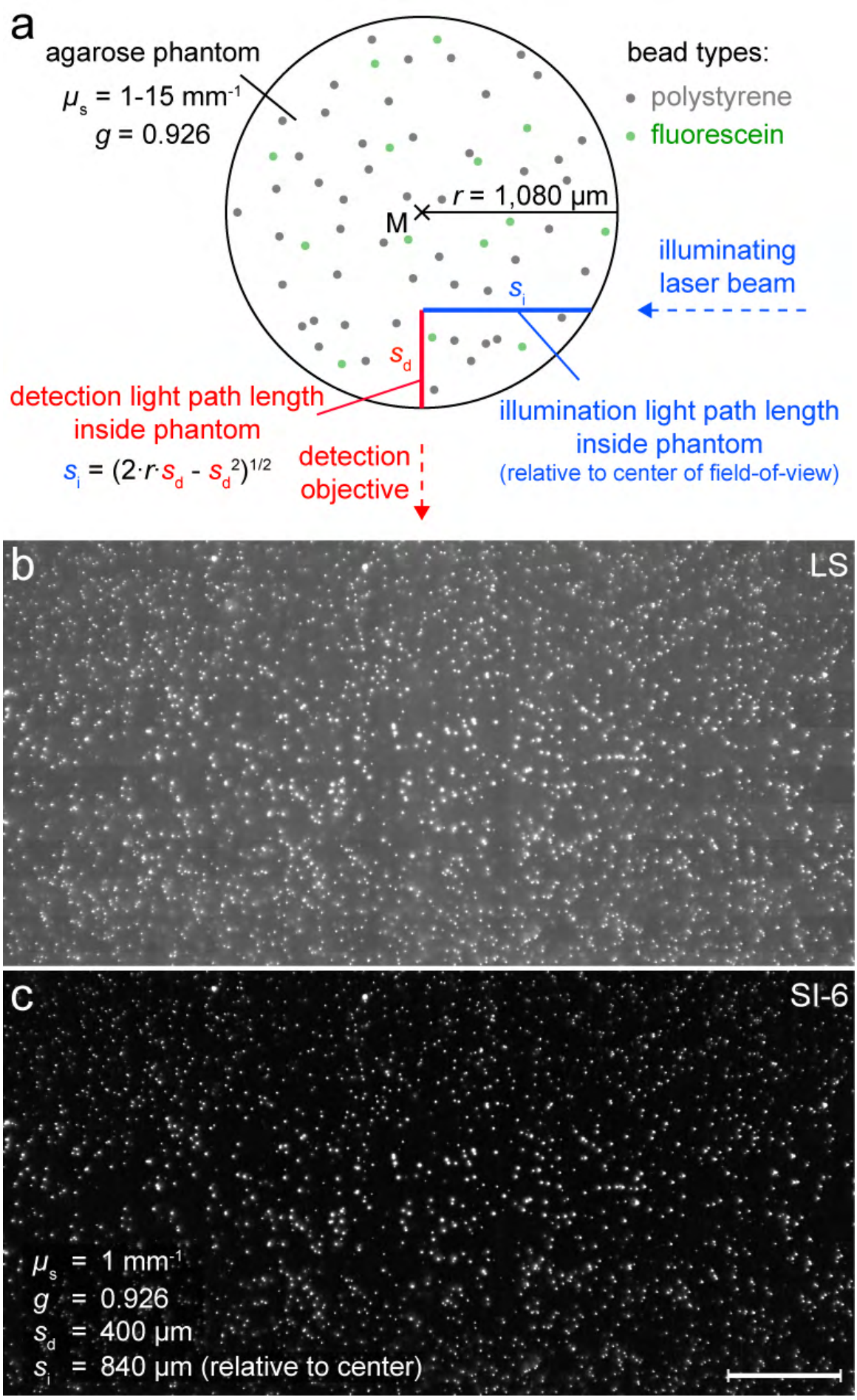

Supplementary Figure 5 | Imaging tissue phantoms with DSLM-SI

(**a**) Sketch of the cross-section of a tissue phantom used to characterize DSLM-SI performance. Fluorescein-containing and non-fluorescent polystyrene latex beads were mixed with low-melting temperature agarose. The mix was allowed to polymerize in a glass capillary with an inner diameter of 2,160 µm. For DSLM-SI imaging, a short section of the agarose cylinder was pushed out of the capillary. The tissue phantom was placed in the water-filled imaging chamber and centered in front of the detection lens. Imaging was performed for phantoms with different scattering coefficients. Contrast enhancement, scattered light removal and penetration depth were analyzed as functions of detection/illumination depth in the cylinder and frequency of the SI illumination pattern (Supplementary Figures 6 and 7). Note that the length of the illumination light path is larger than the length of the detection light path in the cylindrical tissue phantom. Our experimental design allows measurement conditions of multiple scattering in a domain, in which Mie theory applies.

(**b**) Standard DSLM light sheet recording of a single plane in a tissue phantom with scattering coefficient μ_s = 1 mm^{-1}. Laser illumination in (b,c) is from top.

(**c**) DSLM-SI (SI-6) recording of the same plane as in (b). Both panels use the same linear look-up-table, which was adapted for optimal visualization. A comparative quantitative analysis shows that the image contrast in the SI-6 recording is increased by 490 % as compared to the standard light sheet recording. Scale-bar = 50 µm. Carl Zeiss Plan-Apochromat 20×/1.0 W.

Supplementary Figure 6 | DSLM-SI performance at low to intermediate scattering coefficients

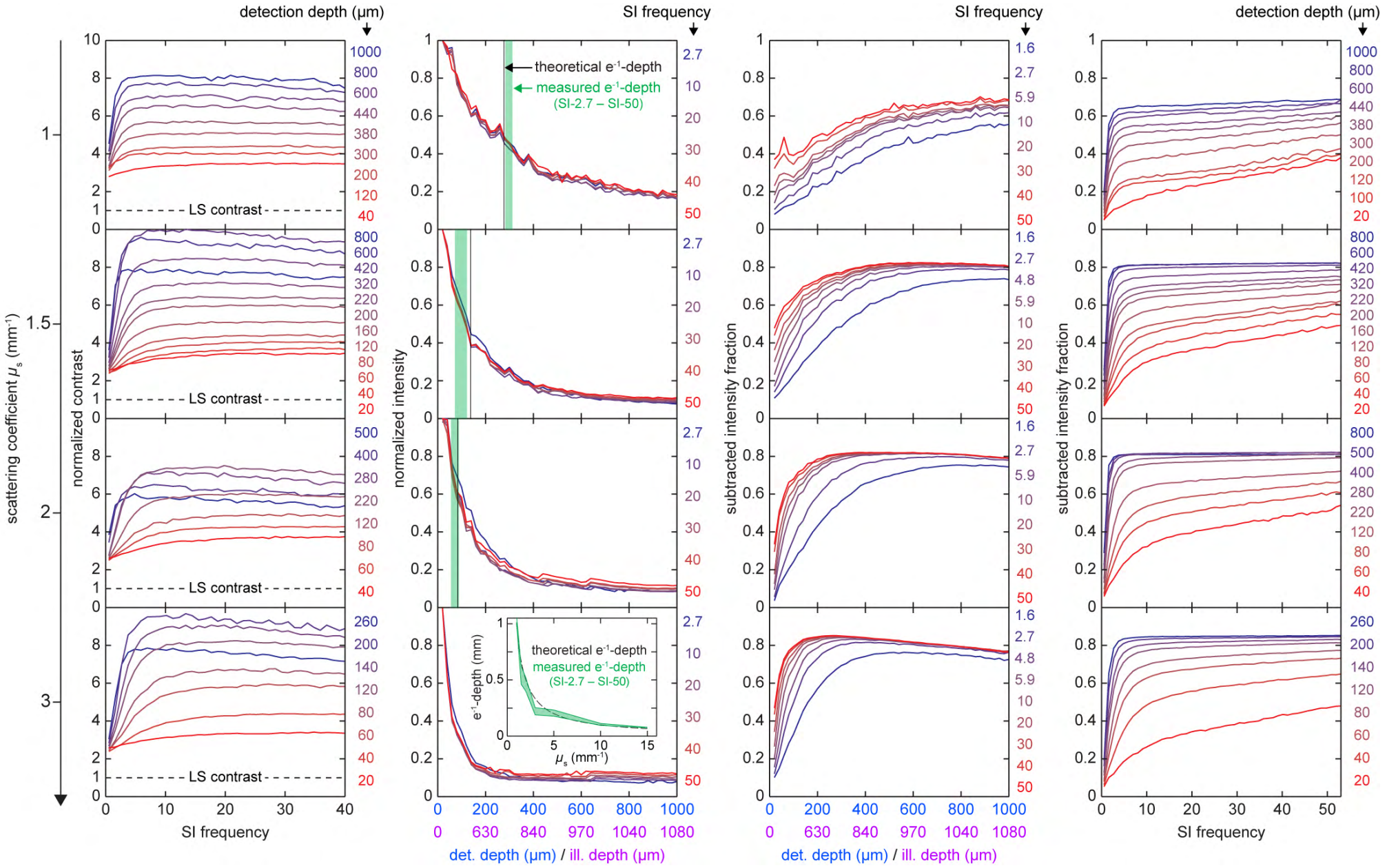

Nature Methods: doi:10.1038/nmeth.1476

Supplementary Figure 6 | DSLM-SI performance at low to intermediate scattering coefficients

Quantification of contrast enhancement (left column), penetration depth (second column from left) and scattering removal in DSLM-SI (right column and second column from right), using tissue phantoms with different scattering coefficients μ_s. DSLM-SI performance was assessed as a function of detection/illumination depth and as a function of the frequency of the SI illumination pattern. An overview of all tissue phantoms is provided in Supplementary Table 1. Scattering coefficients are provided for the illumination wavelength 488 nm. This figure shows results for phantoms A (μ_s = 1 mm^{-1}), B (μ_s = 1.5 mm^{-1}), C (μ_s = 2 mm^{-1}) and D (μ_s = 3 mm^{-1}). Note that phantoms B and C provide scattering coefficients similar to the average values encountered in zebrafish embryonic tissue.

The increase in image contrast arising from the use of DSLM-SI was typically between 150 % and 900 %. The depth-dependent contrast optimum was achieved for SI frequencies between s = 5 (deep inside the phantom) and s = 40 (at the surface of the phantom). The contrast level in the standard DSLM recordings is indicated by the dashed line (reference level for contrast scale).

The green bars in the graphs showing normalized intensity versus detection/illumination depth indicate the measured penetration depths for the entire range of practical SI pattern frequencies (SI-2.7 to SI-50). We fitted the intensity decay and measured an average decrease in penetration depth of 10.6 % for the highest SI frequency as compared to the lowest SI frequency.

Inset (second column from left, bottom panel): Comparison of theoretically expected (black) and measured penetration depths (green, SI-2.7 to SI-50) for the entire range of investigated scattering coefficients. The theoretically expected penetration depths are given by the inverse scattering coefficients and are in good agreement with the measured depths in DSLM-SI.

All phantoms were recorded using identical acquisition settings, laser power levels and optical components (detection lens: Carl Zeiss Plan-Apochromat 20×/1.0 W).

Supplementary Figure 7 | DSLM-SI performance at high scattering coefficients

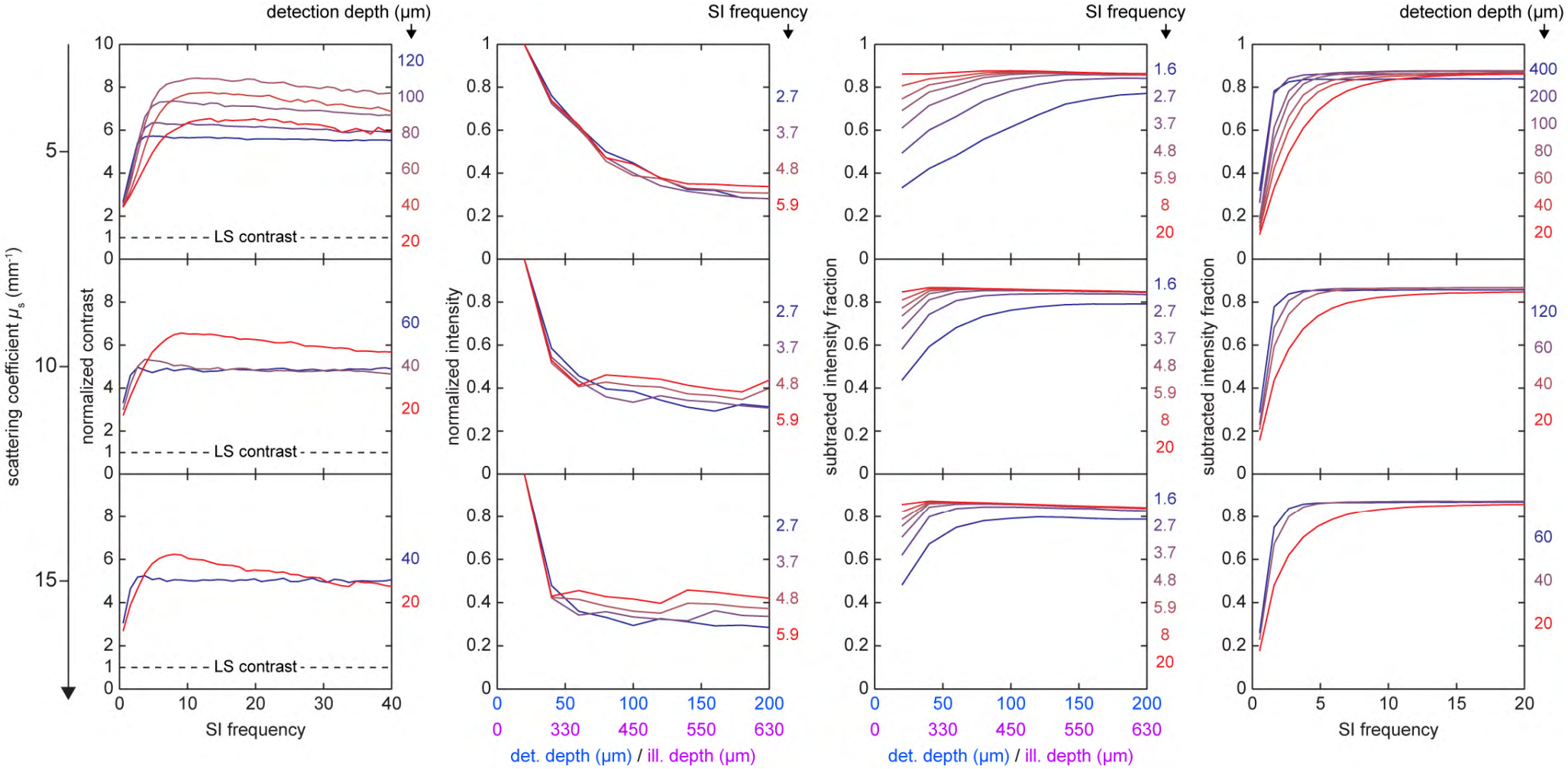

Supplementary Figure 7 | DSLM-SI performance at high scattering coefficients

Quantification of contrast enhancement (left column), penetration depth (second column from left) and scattering removal in DSLM-SI (right column and second column from right), using tissue phantoms with high scattering coefficients (extension of Supplementary Figure 6). DSLM-SI performance was assessed as a function of detection/illumination depth and as a function of the frequency of the SI illumination pattern. An overview of all tissue phantoms is provided in Supplementary Table 1. This figure shows results for phantoms E (μ_s = 5 mm^{-1}), F (μ_s = 10 mm^{-1}), and G (μ_s = 15 mm^{-1}).

Note that phantom E provides a scattering coefficient similar to the average value encountered in *Drosophila* embryonic tissue. No significant change in penetration depth was observed when using different SI frequencies (second column from left).

The increase in image contrast arising from the use of DSLM-SI was typically between 150 % and 700 %. The depth-dependent contrast optimum was achieved for SI frequencies between s = 5 (phantom G) and s = 10-20 (phantom E).

Supplementary Figure 8 | Contrast enhancement in Medaka DSLM-SI recordings

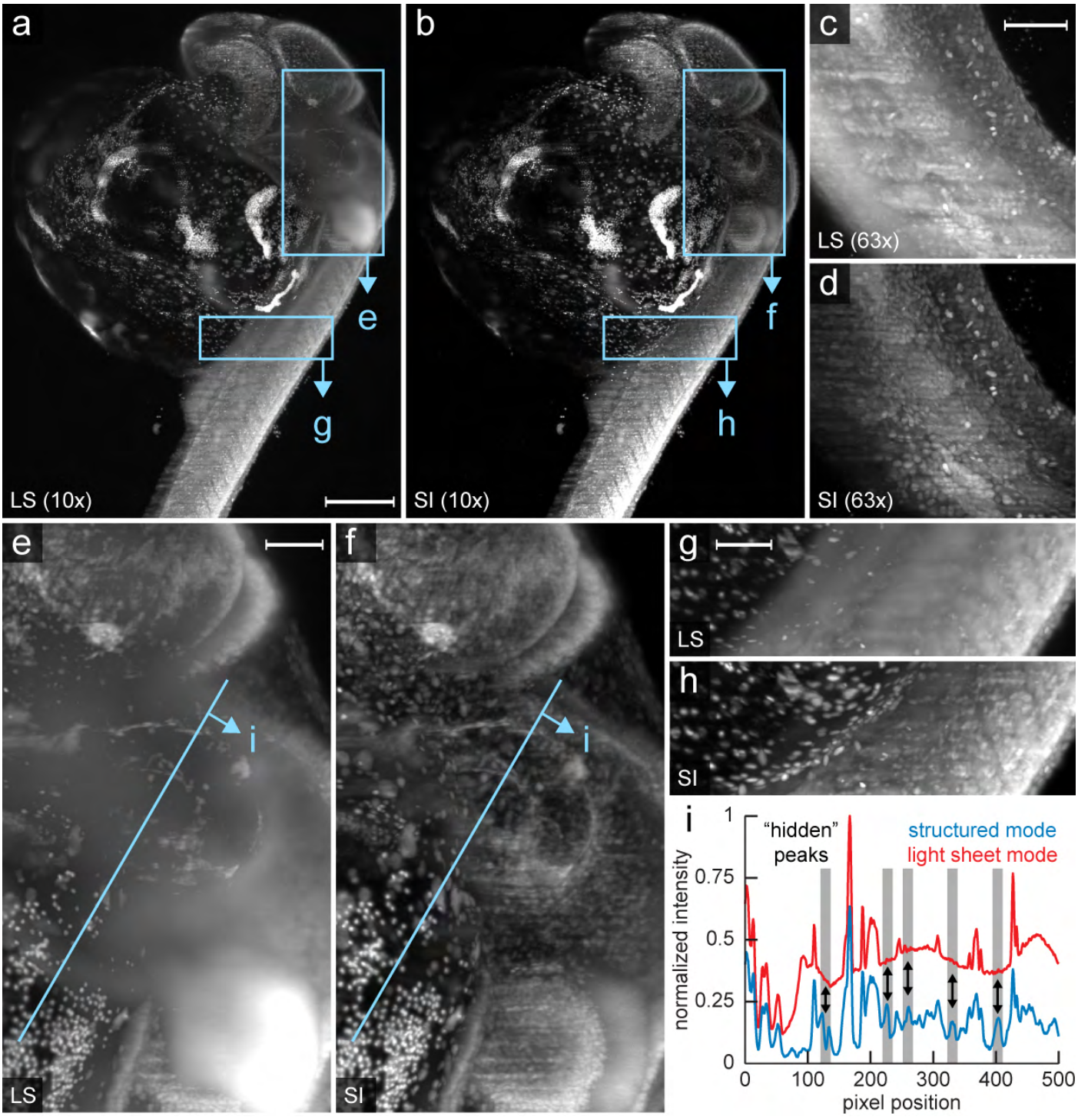

Supplementary Figure 8 | Contrast enhancement in Medaka DSLM-SI recordings

(**a**) Maximum-intensity projection of a DSLM image stack of a 3.5-day old Medaka fish embryo with Sytox Green nuclear staining, recorded with standard light sheet illumination (LS, 10× magnification). Stack dimensions: 435 images, recorded at a z-spacing of 3 µm, covering a total volume of 1,516 × 1,516 × 1,305 µm³. Carl Zeiss C-Apochromat 10×/0.45 W.

(**b**) As in (a), but recorded in structured illumination mode (SI-32). Linear look-up-table from 0 to 4,500 grey levels for panels (a) and (b).

(**c**) Maximum-intensity projection of a DSLM image stack of a 2-day old Medaka fish embryo with Sytox Green nuclear staining, recorded with standard light sheet illumination (LS, 63× magnification). Stack dimensions: 208 images, recorded at a z-spacing of 1.8 µm, covering a total volume of 241 × 241 × 374 µm³. Carl Zeiss Plan-Apochromat 63×/1.0 W.

(**d**) As in (c), but recorded in structured illumination mode (SI-16). Linear look-up-table from 0 to 4,500 grey levels for panels (c) and (d).

(**e**)-(**h**) Close-ups of the regions indicated in (a) and (b). Linear look-up-tables from 50 to 3,000 grey levels for panels (e) and (f), and from 50 to 4,000 for panels (g) and (h).

(**i**) Intensity plot along the line indicated in (e) and (f). In both plots, the raw intensity values are normalized by the same factor (global maximum of both images). Arrows indicate structures in the structured illumination image that are not visible in the light sheet image.

Scale-bars = 200 µm (a,b), 50 µm (c-h). Recording speed: 6 DSLM images per second, 2 SI-reconstructed images per second.

Supplementary Figure 9 | DSLM-SI coverage in zebrafish multi-channel recordings

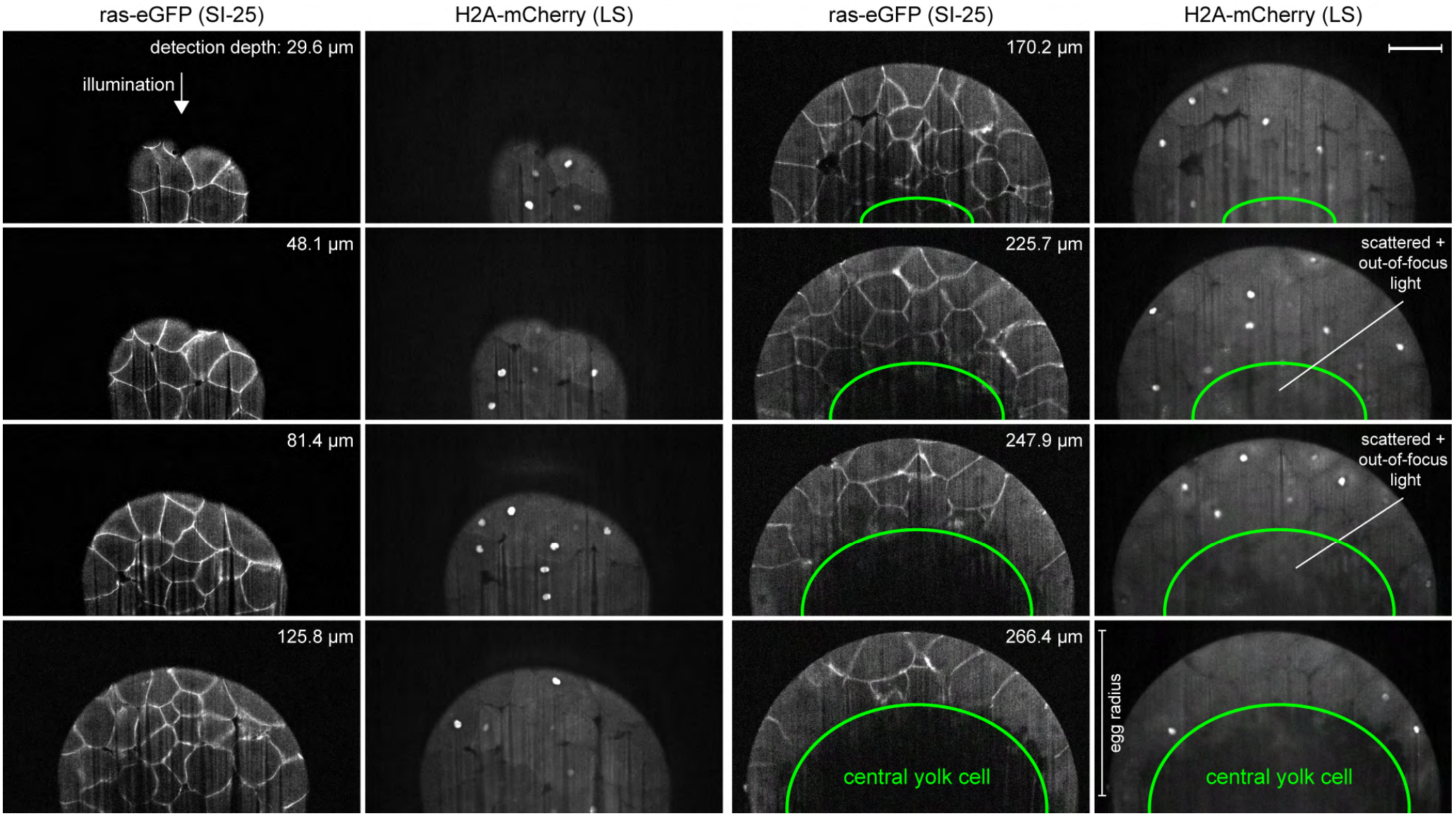

Supplementary Figure 9 | DSLM-SI coverage in zebrafish multi-channel recordings

Single planes from the image stacks recorded at time point 120 min in Supplementary Video 2. The planes are representative of the entire embryo proper, which ends at a detection depth of approximately 300 µm and covers about one-fourth of the surface of the large central yolk cell. Scale-bar = 100 µm (top right frame). Carl Zeiss C-Apochromat 10×/0.45 W.

Supplementary Figure 10 | DSLM-SI coverage at advanced zebrafish embryonic development

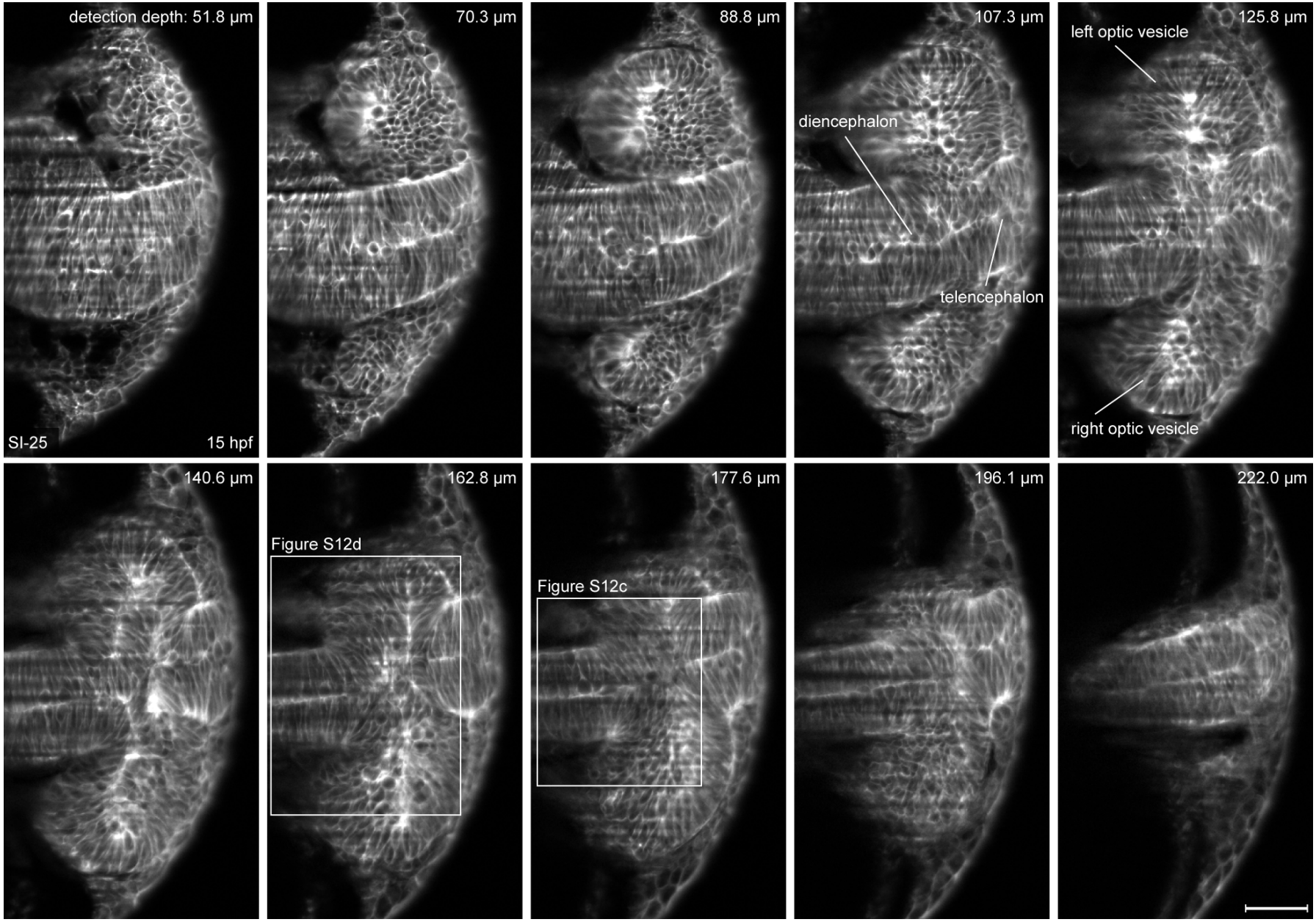

Nature Methods: doi:10.1038/nmeth.1476

Supplementary Figure 10 | DSLM-SI coverage at advanced zebrafish embryonic development

Single planes from the DSLM-SI image stack recorded at time point 15 h.p.f. in Supplementary Video 3. The planes show the entire head of the embryo, including forebrain, midbrain and both optic vesicles. Scale-bar = 50 µm. Carl Zeiss C-Apochromat 10×/0.45 W.

Supplementary Figure 11 | DSLM-SI coverage at late zebrafish embryonic development

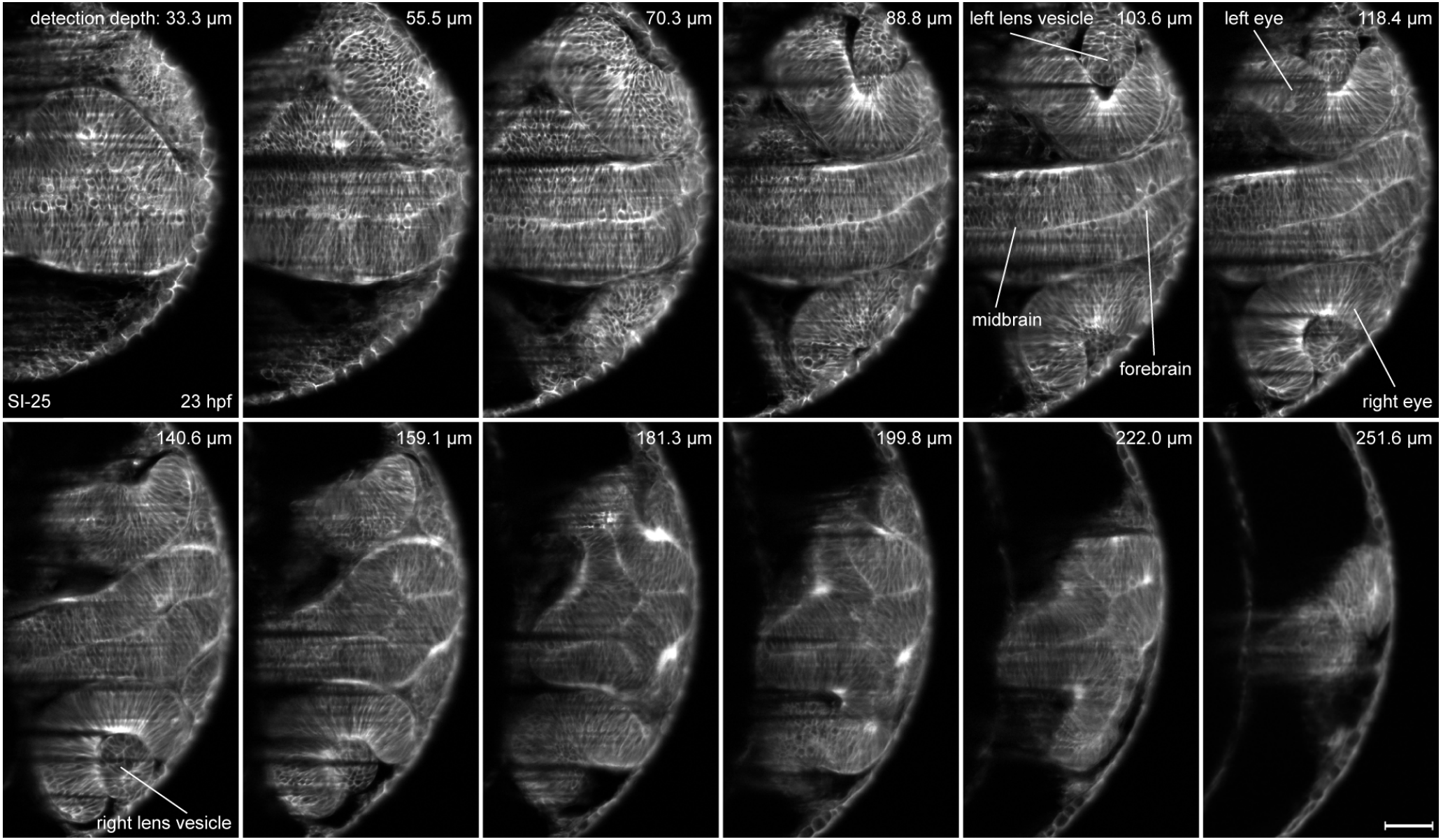

Nature Methods: doi:10.1038/nmeth.1476

Supplementary Figure 11 | DSLM-SI coverage at late zebrafish embryonic development

Single planes from the DSLM-SI image stack recorded at time point 23 h.p.f. in Supplementary Video 3. The planes show the entire head of the embryo, including forebrain, midbrain and both eyes. Scale-bar = 50 µm. Carl Zeiss C-Apochromat 10×/0.45 W.

Supplementary Figure 12 | Removal of scattered light in zebrafish DSLM-SI recordings

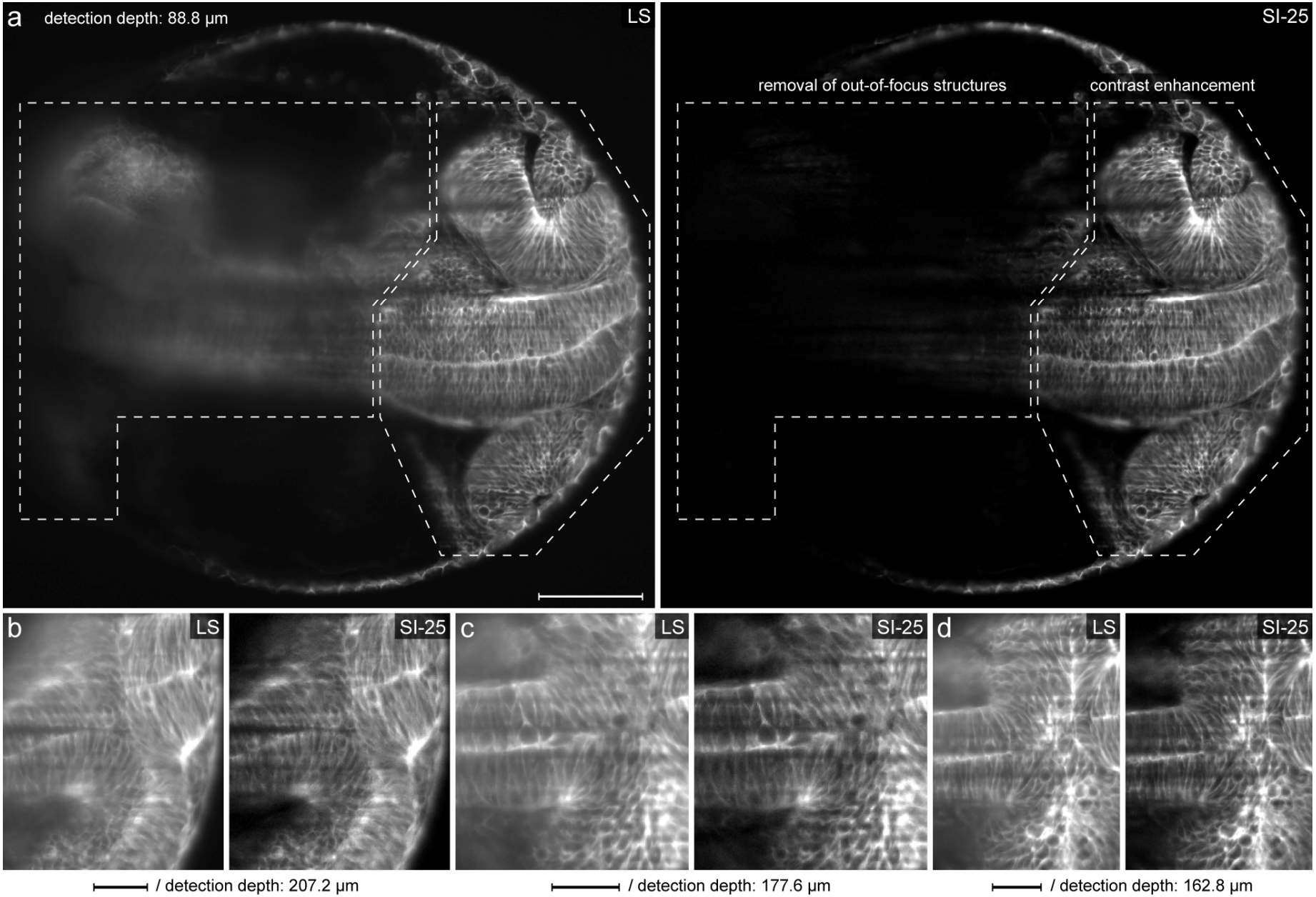

Supplementary Figure 12 | Removal of scattered light in zebrafish DSLM-SI recordings

Comparison of single planes from standard light sheet (left) and DSLM-SI (right) recordings of the zebrafish shown in Supplementary Video 3. Carl Zeiss C-Apochromat 10×/0.45 W.

(**a**) Comparison of entire images at a detection depth of 88.8 µm. Note that the 23-hour-old embryo bends around the 700-µm-large central yolk cell, which cannot be penetrated with the light microscope. Therefore approximately half of the embryo shown in this frame is located in the shadowed region behind the yolk (left part). The illuminating laser light beam, which enters the specimen from the right, also reaches those parts, but the light is heavily scattered and produces a very low-contrast image of this section of the embryo. Moreover, the laser beam is refracted at the embryo-proper/yolk interface, such that the standard light sheet image shows both in-focus and out-of-focus structures of the embryo. DSLM-SI selectively removes all out-of-focus structures and increases the contrast for the in-focus structures (here: 42.4 % increase in contrast). Scale-bar = 100 µm.

(**b**)-(**d**) Comparison of standard light sheet (LS) and DSLM-SI recordings at different depths and different time points in development (b: 17 h.p.f.; c,d: 15 h.p.f.) for the same data set (Supplementary Video 3). The increase in image contrast in DSLM-SI is 74.3 % (b), 91.1 % (c) and 81.7 % (d), respectively. These numbers quantify only the contrast enhancement for in-focus structures. An additional feature of DSLM-SI is the complete removal of out-of-focus structures as shown in (a). Scale-bars = 40 µm.

Supplementary Figure 13 | Removal of scattered light in *Drosophila* DSLM-SI recordings

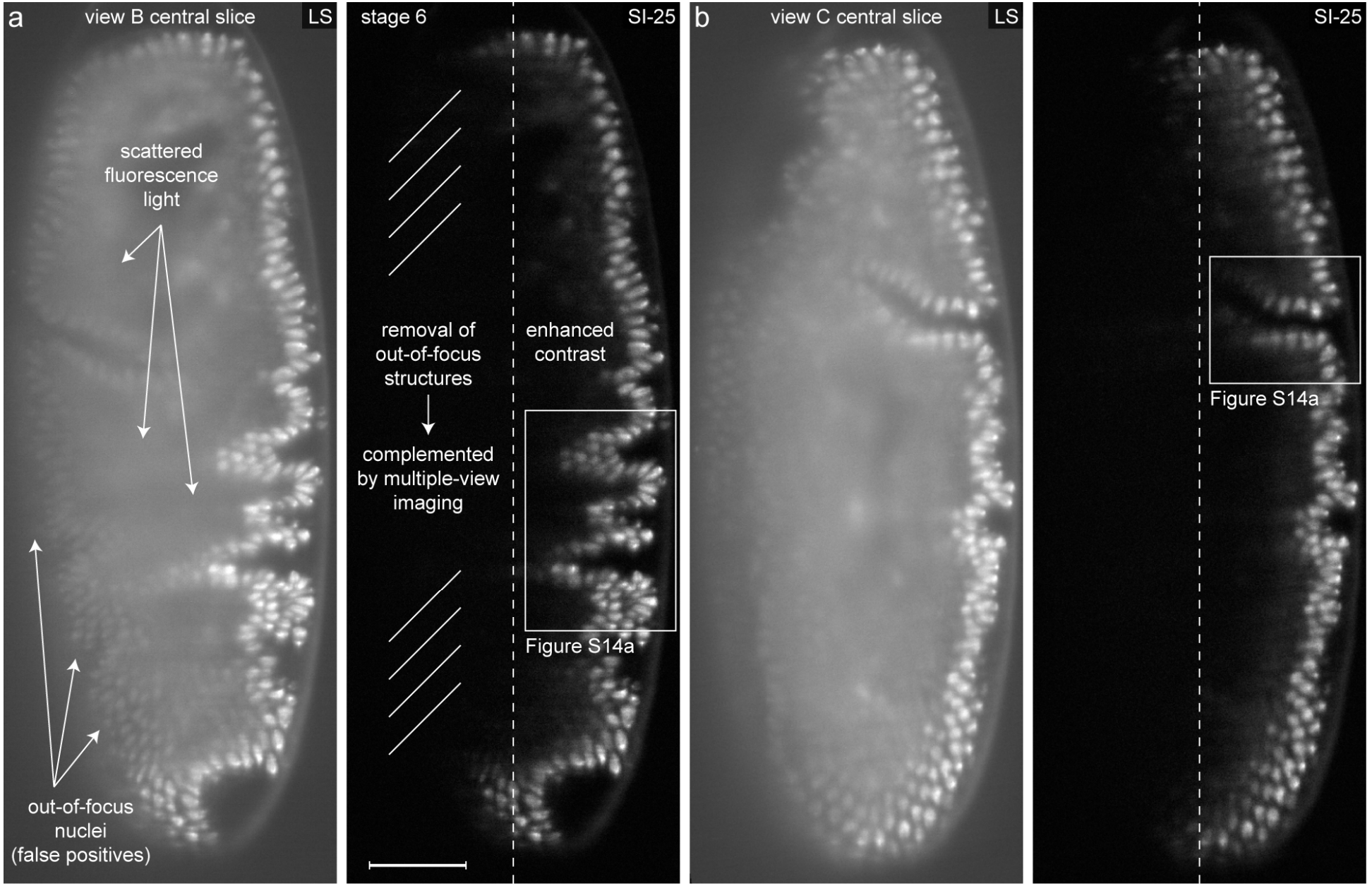

Supplementary Figure 13 | Removal of scattered light in *Drosophila* DSLM-SI recordings

Demonstration of the two main advantages of DSLM-SI – removal of out-of-focus structures and contrast enhancement for in-focus structures – in the imaging of early *Drosophila* development. The panels show a comparison of single planes from standard light sheet (LS) and DSLM-SI recordings. The four images represent two views from our four-view recording shown in Supplementary Video 4. The combination of DSLM-SI and DSLM multiple-view imaging maximizes the image contrast throughout the specimen, eliminates false positives in the data analysis (such as out-of-focus nuclei, i.e. structures that are represented more than once at seemingly different locations within the same multiple-view data set) and ensures maximum coverage of the observed specimen at the same time. The increase in image contrast arising from DSLM-SI is 260.8 % in (a) and 261.5 % in (b), respectively.

Note that a stage 6 *Drosophila* embryo has not yet developed internal structures. The signal in the central parts of the standard light sheet recordings represents scattered background light arising from out-of-focus structures.

(**a**) Central slices from view B at stage 6. At this imaging depth, the incident laser beam (from the right) enters the embryo under an angle of 45 ° to the surface of the approximately ellipsoidal shape of the embryo. Since the lengths of the illumination and detection light paths in the specimen are identical in this scenario, the selected images are well-suited to quantify the penetration depth into the embryo (see Supplementary Figure 14a).

(**b**) Central slices from view C at stage 6. This view shows the embryo at an angle perpendicular to view B. Note the presence of out-of-focus nuclei on the left-hand side of the standard light sheet (LS) image.

Scale-bar = 50 µm. Carl Zeiss Plan-Apochromat 20×/1.0 W.

Supplementary Figure 14 | DSLM-SI penetration depth in early *Drosophila* embryogenesis

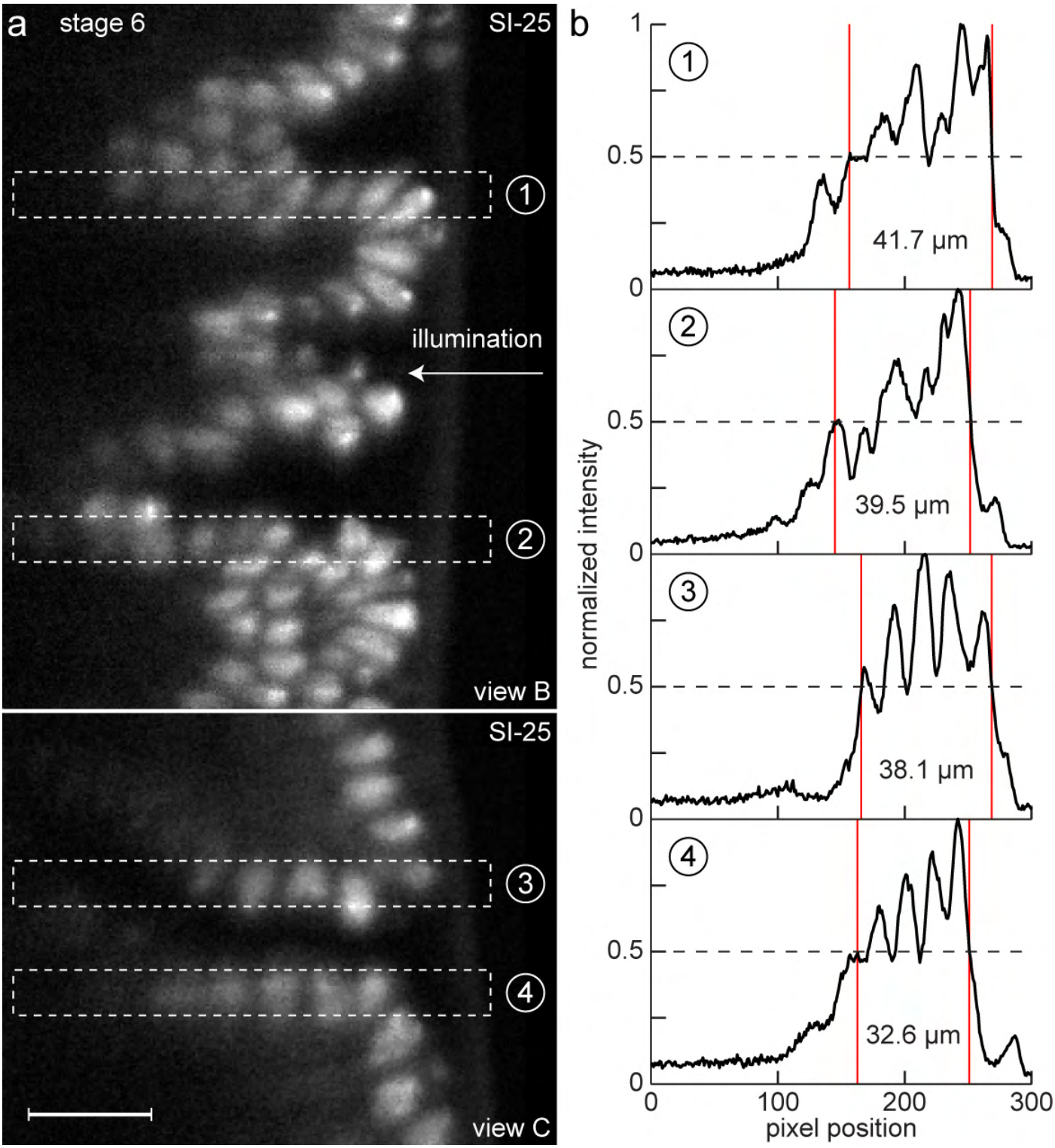

Supplementary Figure 14 | DSLM-SI penetration depth in early *Drosophila* embryogenesis

(**a**) Close-ups of the DSLM-SI images shown in Supplementary Figure 13. The images represent central slices of the respective views, i.e. they show fluorescence data at an imaging depth, at which the illuminating laser beam enters the almost rotationally symmetrical specimen under 45 °. In this scenario, the lengths of the illumination and detection light paths in the specimen are identical and the measured penetration depths can be directly compared to data obtained from confocal and two-photon fluorescence microscopes. Scale-bar = 20 µm. Carl Zeiss Plan-Apochromat 20×/1.0 W.

(**b**) Intensity profiles along the rectangles indicated in (a). One pixel corresponds to 370 nm in the specimen. Pixel positions close to 300 correspond to surface regions (vitelline membrane). The intensity profiles reveal an average penetration depth of 38.0 ± 3.8 µm (50% signal decay) in the DSLM-SI images of the stage 6 *Drosophila* wild-type embryo. The value we obtained for DSLM-SI is slightly higher than values previously reported for conventional two-photon fluorescence microscopy at stages 5 and 8 for the same type of specimen (Supatto *et al.* 2009, *Nature Protocols*, Figure 2e). Note that our value of 38.0 ± 3.8 µm represents an underestimate of the real penetration depth, since the embryo has not yet developed internal structures. In particular, there are no histone-eGFP labeled structures at pixel positions 0-100 and, thus, no direct signal can contribute to the intensity levels measured for these pixels.

Supplementary Figure 15 | Workflow for processing and visualization of DSLM-SI recordings

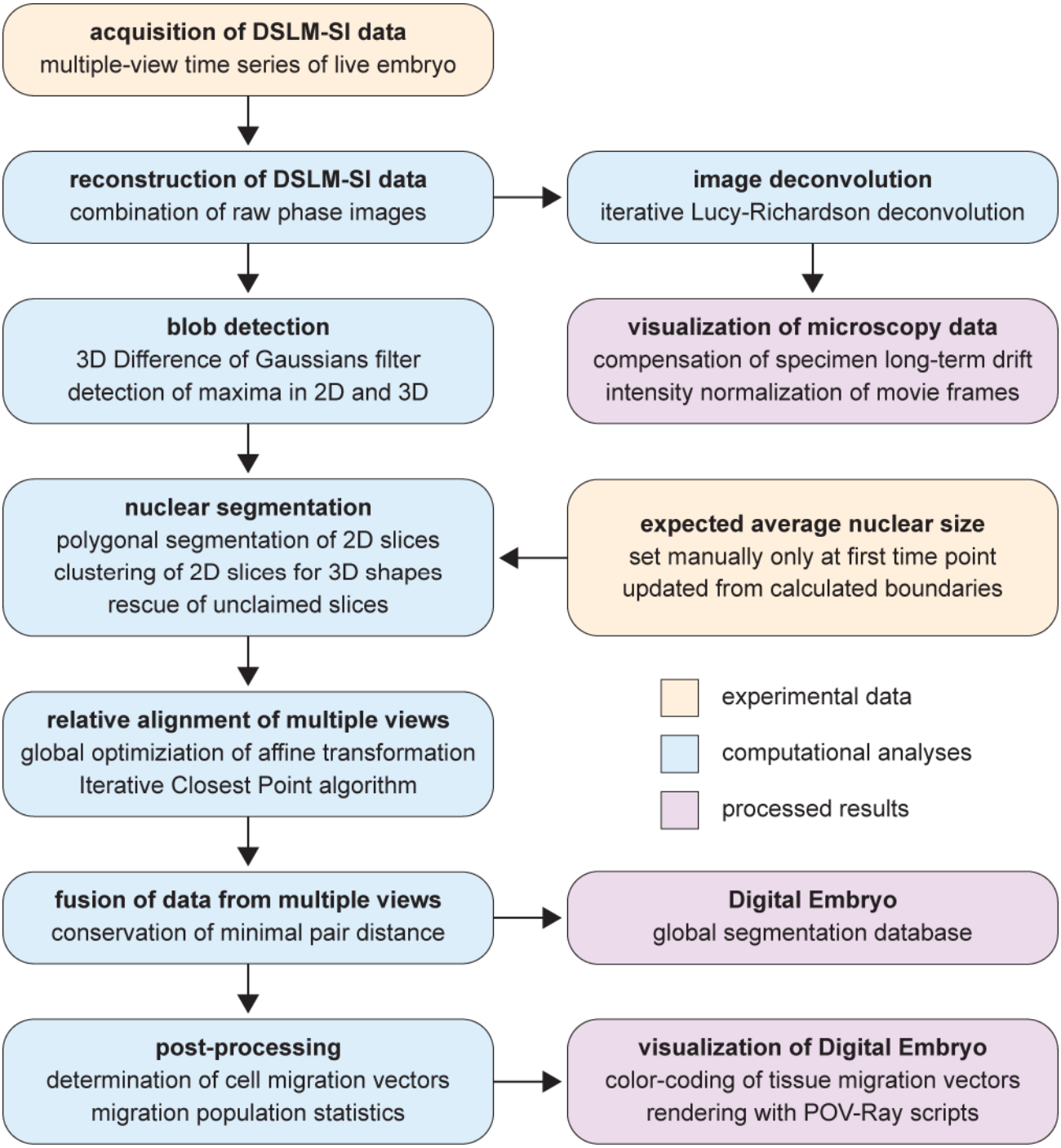

Supplementary Figure 15 | Workflow for processing and visualization of DSLM-SI recordings

Schematic workflow for the analysis of DSLM-SI recordings. The steps “acquisition of DSLM-SI data”, “reconstruction of DSLM-SI data”, “image deconvolution” and “visualization of microscopy data” are typically performed on all data sets. This part of the pipeline was used to create Supplementary Videos 2-4. All other steps are specific to the reconstruction of cell positions in nuclei-labeled *Drosophila* multiple-view time-lapse recordings and summarize the processing underlying Supplementary Videos 5 and 6. Note that the step “image deconvolution” is used exclusively for visualization purposes. All quantitative analyses, such as the reconstruction of the *Drosophila* Digital Embryo, were performed directly on the raw data to exclude potential data bias.

Supplementary Figure 16 | Multiple-view fusion of the *Drosophila* Digital Embryo

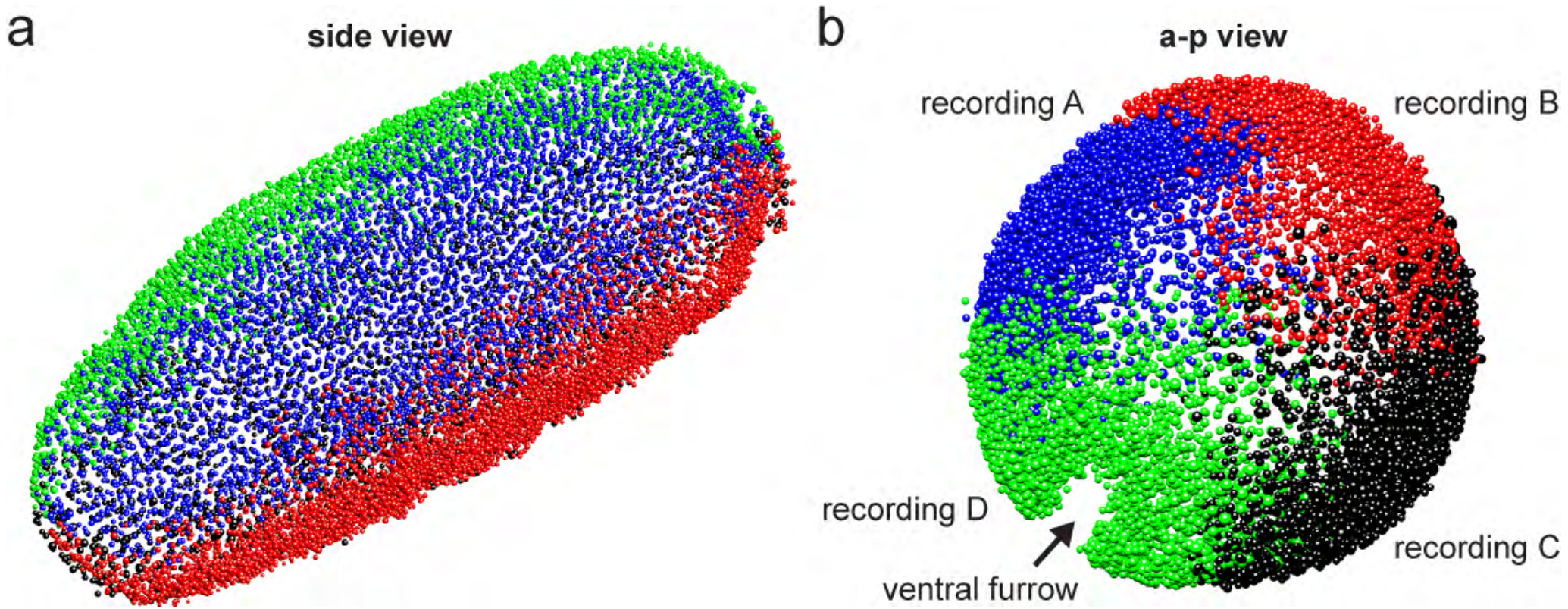

Nature Methods: doi:10.1038/nmeth.1476

Supplementary Figure 16 | Multiple-view fusion of the *Drosophila* Digital Embryo

Alignment of the four point clouds representing the nuclei detected in the four views of the developing *Drosophila* embryo. Nuclei shown in different colors originate from different microscopic views. (a) Side view and (b) view along the anterior-posterior axis of the embryo for one time point in Supplementary Video 5.

Supplementary Table 1 | Properties of tissue phantoms

phantom	μ_s [mm^{-1}]	g	c_{beads} [ml^{-1}]	$v_{f\text{-}beads}$ [µl]	$v_{p\text{-}beads}$ [µl]	v_{agar} [µl]
A	1	0.9261	1.059×10^9	8.78	0	991.22
B	1.5	0.9261	1.588×10^9	8.78	4.74	986.48
C	2	0.9261	2.117×10^9	8.78	9.58	981.64
D	3	0.9261	3.176×10^9	8.78	18.96	972.26
E	5	0.9261	5.293×10^9	8.78	37.91	953.31
F	10	0.9261	1.059×10^{10}	8.78	85.29	905.93
G	15	0.9261	1.588×10^{10}	8.78	132.67	858.55

The tissue phantoms were created by adding fluorescein-containing polystyrene latex beads (Polysciences, Fluoresbrite Plain YG 0.75 µm, stock concentration 1.206×10^{11} ml^{-1}) and non-fluorescent polystyrene latex beads (Polysciences, Polybead Polystyrene 0.75 µm, stock concentration 1.117×10^{11} ml^{-1}) to 1.5 % low-melting temperature agarose. The table provides an overview of the most relevant optical properties of the phantoms (scattering coefficient μ_s, average cosine of phase function g, concentration of beads c_{beads}) as well as information on their preparation (volume of fluorescent bead stock solution $v_{f\text{-}beads}$, volume of non-fluorescent bead stock solution $v_{p\text{-}beads}$, agarose volume v_{agar}). The optical properties were calculated using Mie theory, assuming a sphere diameter of 711 nm, a vacuum wavelength of 488 nm, a refractive index of 1.33 for the medium and a real index of 1.55 for the spheres.

Supplementary Data: The public *Drosophila* Digital Embryo database

We provide public access to the Digital Embryo Databases included in this study. The online repository comprises data sets with the three-dimensional positions, diameters and fluorescence intensity levels of the nuclei reconstructed from the DSLM-SI recording of *Drosophila* wild-type development (presented in Supplementary Video 4), as well as all movies associated with this study. The databases and movies are accessible at http://www.digital-embryo.org.

Each of the two Digital Embryo Databases is provided as a Matlab MAT-file, containing a multi-cell array. Each Matlab cell corresponds to one time point and contains a two-dimensional table characterizing the nuclei segmented at the respective time point. Each row corresponds to one nucleus and includes the following parameters:

Columns 1-3:	x-y-z coordinates of the center-of-mass of the nucleus (length unit = 370 nm)
Column 4:	Diameter of the sphere matching the volume occupied by the nucleus
Column 5:	Average fluorescence intensity of the nucleus (arbitrary units)
Column 6:	Index of the microscopic view the nucleus originates from (only applicable to the raw reconstruction of the multiple-view data set; indices 1-4 correspond to views 0 °/90 °/180 °/270 °)

Specifications of the two data sets provided in the public database:

- **Data Set 1:** *Raw reconstruction of early Drosophila wild-type development*
  Filename: "drosophila_raw.mat"
  Number of time points and temporal sampling:
  191 time points (120-690 m.p.f.), 180-sec-intervals
  Number of nucleus entries: 3,624,857 (49.5 MB)
  Related manuscript items: Figures 3a/b, S13-S16; Supplementary Videos 4, 5

- **Data Set 2:** *Fused reconstruction of early Drosophila wild-type development*
  Filename: "drosophila_fused.mat"
  Number of time points and temporal sampling:
  191 time points (120-690 m.p.f.), 180-sec-intervals
  Number of nucleus entries: 1,486,971 (20.5 MB)
  Related manuscript items: Figures 3a-c, S13-S16; Supplementary Videos 4, 6